Rock and Soil Mechanics

Volume 43 | Issue 10 Article 7

11-25-2022

Three-dimensional stability limit analysis of cracked loess slopes

Xue-liang ZHU
Institute of Geotechnical Engineering, Xi'an University of Technology, Xi'an, Shaanxi 710048, China

Sheng-jun SHAO
Shaanxi Key Laboratory of Loess Mechanics and Engineering, Xi'an University of Technology, Xi'an, Shaanxi 710048, China

Xiao-jun SHEN
Hanjiang to Weihe River Valley Water Diversion Project Construction Co., Ltd., Xi'an, Shaanxi 710000, China

Shuai SHAO
Department of Architecture and Urban Planning, Xi'an University of Technology, Xi'an, Shaanxi 710048, China, shaoshuai@xaut.edu.cn

See next page for additional authors

Custom Citation

ZHU Xue-liang, SHAO Sheng-jun, SHEN Xiao-jun, SHAO Shuai, LIU Xiao-kang, . Three-dimensional stability limit analysis of cracked loess slopes[J]. Rock and Soil Mechanics, 2022, 43(10): 2735-2743.

Three-dimensional stability limit analysis of cracked loess slopes

Authors

Xue-liang ZHU, Sheng-jun SHAO, Xiao-jun SHEN, Shuai SHAO, and Xiao-kang LIU

Rock and Soil Mechanics 2022 43(10): 2735−2743 ISSN 1000−7598
https: //doi.org/10.16285/j.rsm.2021.7080 rocksoilmech.researchcommons.org/journal

Three-dimensional stability limit analysis of cracked loess slopes

ZHU Xue-liang[1], SHAO Sheng-jun[1, 2], SHEN Xiao-jun[3], SHAO Shuai[4], LIU Xiao-kang[1]

1. Institute of Geotechnical Engineering, Xi'an University of Technology, Xi'an, Shaanxi 710048, China
2. Shaanxi Key Laboratory of Loess Mechanics and Engineering, Xi'an University of Technology, Xi'an, Shaanxi 710048, China
3. Hanjiang to Weihe River Valley Water Diversion Project Construction Co., Ltd., Xi'an, Shaanxi 710000, China
4. Department of Architecture and Urban Planning, Xi'an University of Technology, Xi'an, Shaanxi 710048, China

Abstract: The development of vertical cracks in loess slopes often affects slope stability. Compared with the plane strain mechanism, the slope stability analysis under the three-dimensional (3D) failure mechanism is closer to the actual slope instability. Based on the upper bound method of plastic limit analysis, different failure mechanisms (face failure, toe failure and base failure) of 3D loess slope with pre-existing cracks are considered, the energy balance equation and its dimensionless critical height expression $\gamma H/c$ are established, and the upper bound solution of critical height is obtained by random search method. The effects of constraint width, slope angle, internal friction angle and crack depth on the critical height of 3D vertical cracked loess slopes are analyzed. The results indicate that for the toe failure mechanism, the critical height decreases with the increase of crack depth, and the increase in crack depth no longer affects the critical height after reducing to the critical crack depth $(\delta/H)_{\min}$. The critical crack depth increases with the increase of slope angle β and decreases with the increase of internal friction angle φ. When the constraint width B/H<0.8, most of the failure mechanism is of face failure. When the constraint width B/H=0.8, internal friction angle φ=10°, and the constraint width B/H=0.6, internal friction angle φ=15°, the failure mechanism of the slope gradually transits from the face failure mechanism to the toe failure mechanism. The loess slope with vertical cracks has a smaller critical height than the intact slope. The constraint width and internal friction angle can affect the failure mechanism of 3D loess slopes.

Keywords: slope instability; vertical cracks; failure mechanism; upper bound method

1 Introduction

Slope stability is one of the three classical engineering practical problems in geotechnics. Many scholars have conducted in-depth research on it in the past, and the methods usually used for slope stability analysis are divided into three categories: limit equilibrium method, limit analysis method and numerical analysis method[1]. The limit equilibrium method is an analysis method based on static equilibrium, which has a simple theoretical basis and is widely used. Still, there are some shortcomings: it fails to take into account the stress−strain relationship of soil and requires more assumptions, which makes it different from the actual situation. Numerical analysis methods (such as finite element method and discrete element method) have the problems of cumbersome modeling and difficulty in determining the basis of instability, although different types of constitutive relationships can be considered. The limit analysis method is a method premised on plastic mechanics, which can take into account the plasticity of soil and establish the equilibrium relationship through the upper and lower bound theorem to obtain the limit solution of the slope stability problem

Cracks are usually found at the top of loess slopes, and the existence of cracks will lead to a significant reduction in slope stability. Slope cracks are generally divided into two categories: one is the cracks generated under the influence of climatic factors, and the cracks at the slope crest occur before the slope failure, which is called "pre-existing crack"; the other type is the cracks generated during the slope failure, which are called "crack in the formation process"[2]. Chen[3] proposed a log-spiral failure mechanism under plane strain and used limit analysis theory to study the stability of rock and soil slopes. Spencer[4] studied the introduction of tension cracks in the circular failure mechanism and derived the equation for crack depth, and obtained that the crack depth was affected by soil weight, cohesion and internal friction angle. Michalowski[5] and Utili[2] proposed stability analysis methods for slopes with cracks under the framework of limit analysis theory in order to gain insight into the influence of cracks on slope stability problems and obtained the influence of crack depth as well as the crack location

Received: 9 December 2021 Revised: 22 June 2022
This work was supported by the National Natural Science Foundation of China (52108342), the Shaanxi Province Natural Science Foundation Research Program–Hanjiang-Weihe Joint Fund Project (2019JLP-21, 2019JLZ-13), the Ph.D. Launch Fund of Xi'an University of Technology (107-451122001) and the Shaanxi Water Science and Technology Program (2021slkj-12).
First author: ZHU Xue-liang, male, born in 1996, Master degree candidate, mainly engaged in the loess mechanics and limit analysis of slope stability. E-mail: 3406313594@qq.com
Corresponding author: SHAO Shuai, male, born in 1990, PhD, Lecture, mainly engaged in the loess mechanics. E-mail: shaoshuai@xaut.edu.cn

on the slope stability, which provided references for subsequent analysis methods for slopes with cracks. Most of previous studies on the slope stability have been conducted under two-dimensional plain strain conditions, however, the two-dimensional analysis are often on the conservative side. Additionally, it can be observed that the natural slope failure has a three-dimensional characteristic and a crack development characteristic. Therefore, ignoring the influence of three-dimensional characteristics of slope failure and the impact of crack development will lead to a conservative result in the slope stability analysis.

Michalowski and Drescher[6] proposed the horn-shape three-dimensional failure mechanism, and then Gao et al.[7] extended the three-dimensional slope failure mode (face failure and base failure) on this basis. He et al.[8] established the three-dimensional failure mechanism of cracked slopes and concluded that with the increase in slope width, the impact of the most critical crack on the slope stability decreased significantly. He et al.[9] further considered the stability of cracked slopes with upper slope inclinations and obtained that with the increase of upper slope inclination, the critical crack depth would gradually increase and its position would deviate more and more from the crest. Li et al.[10] adopted the pseudo-static method to consider the stability of three-dimensional slopes under seismic loading and obtained that the seismic response would greatly reduce the slope stability, which was consistent with our perception. Rao et al.[11] used the Monte Carlo simulation method and mode search method to analyze the three-dimensional stability of cracked slopes under different failure modes, and the influence of cracks on the slopes was studied.

Since there are few pieces of literature on the stability analysis of cracked slopes, this paper mainly investigates the stability of three-dimensional homogeneous loess slopes under three failure modes (face failure, toe failure and base failure), based on the upper bound limit analysis and the random search method proposed by Chen[12].

2 Rotational failure mechanism for cracked slopes

2.1 Log-spiral failure mechanism

Slope failure mechanisms commonly include the translational failure mechanism (the sliding surface is planar), the rotational failure mechanism (the sliding surface is circular), and the translational-rotational failure mechanism. For a generally assumed slope sliding surface, the kinematically admissible velocity field is constructed based on the upper bound theory of limit analysis. Chen[3] assumed a slope sliding surface rotating around the pole in the limit state in his monograph and proposed a log-spiral failure mechanism according to the Mohr-Coulomb criterion and associated flow rule. Michalowski and Drescher[6] extended the two-dimensional failure mechanism to a horn-shape three-dimensional failure mechanism based on Chen's method, as shown in Fig. 1.

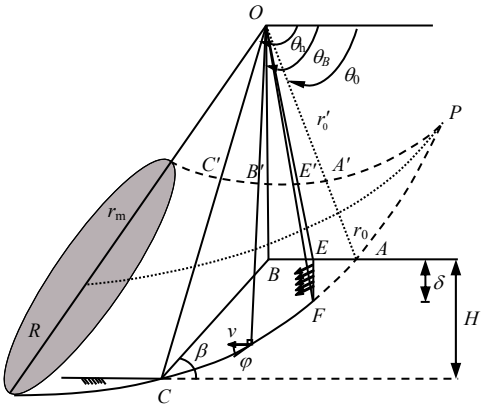

Fig. 1 Three-dimensional rotational failure mechanism of cracked slopes

The equation of the curve PAC is

$$r(\theta) = r_0 \mathrm{e}^{(\theta-\theta_0)\tan\varphi} \tag{1}$$

The equation of the curve $PA'C'$ is

$$r'(\theta) = r_0' \mathrm{e}^{-(\theta-\theta_0)\tan\varphi} \tag{2}$$

where $r(\theta)$ and $r'(\theta)$ are the radius distances from a point on the log-spiral to the pole O; θ is the angle between the horizontal reference line and the radius of the line where it is located; r_0 and r_0' are respectively OA and OA' in Fig. 1, which are equivalent to the radii of the angle θ_0; and φ is the soil internal friction angle.

It is known from the principle of virtual work that the work rate done by the external force is equal to the work rate of energy dissipation in the velocity field (i.e., failure mechanism) established for the arbitrary admissible velocity field[3], i.e.,

$$\int_V \boldsymbol{\sigma}_{ij}\, \dot{\varepsilon}_{ij}^{*}\, \mathrm{d}V = \int_A T_i\, \dot{u}_i^{*}\, \mathrm{d}A + \int_V F_i\, \dot{u}_i^{*}\, \mathrm{d}V \tag{3}$$

where A and V are respectively the area and the volume over the entire integral object domain; T_i is the surface force; F_i is the body force; u_i^* is the kinematically admissible velocity field; ε_{ij}^* is the strain rate in the kinematically admissible velocity field; and $\boldsymbol{\sigma}_{ij}$ is the stress tensor corresponding to the strain rate.

2.2 Failure mode of three-dimensional cracked slopes

Most of the cracks existing in loess slopes are developped along the vertical direction, which makes the slope exhibit an obvious three-dimensional effect[13] when the slope width is constrained during failure.

Therefore, it is necessary to study the stability analysis method of three-dimensional cracked loess slopes. According to Gao et al.[7], the three-dimensional rotational failure mechanism of earth slopes has been extended from the toe failure to the face failure and the base failure. By analogy with their calculation and analysis method, in this paper the stability of three-dimensional loess slopes with vertical cracks is considered under different failure modes, namely, toe failure, face failure and base failure, as shown in Fig. 2.

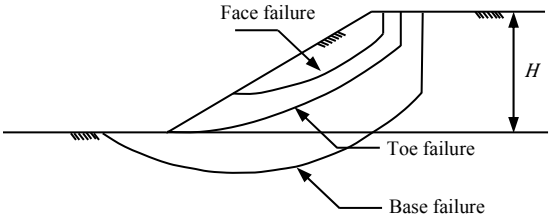

Fig. 2 Three types of failure mechanism for cracked slopes

3 Equilibrium equations for different failure modes

In this paper, the study of three-dimensional homogenous loess slopes with vertical cracks under different failure mechanisms is carried out based on the kinematic analysis of limit analysis. In order to let the three-dimensional failure mechanism degrade to the log-spiral failure mechanism under plane strain when the width tends to infinity, as shown in Fig. 3, a block is inserted on the symmetry plane. The plane insert is a log-spiral under plane strain with a width of b, forming a failure mechanism combined with the middle plane insert and the curvilinear cone at the two symmetric ends.

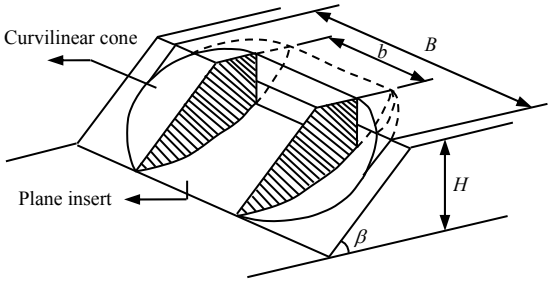

Fig. 3 Three-dimensional rotational failure mechanism with crack (with plane insert)

3.1 Face failure mechanism

For the failure mode of three-dimensional loess slopes with cracks, the three-dimensional face failure mechanism (see in Fig. 4) is very similar to the three-dimensional toe failure mechanism (see in Fig. 1). Therefore, similar to the method proposed by Gao et al.[7], $n = H'/H$ is introduced. When $n = 1$, the three-dimensional toe failure mechanism is a special case of the three-dimensional face failure mechanism. δ can be introduced to represent the crack EF, whose location is determined by the angles θ_E and θ_F, as shown in Fig. 4.

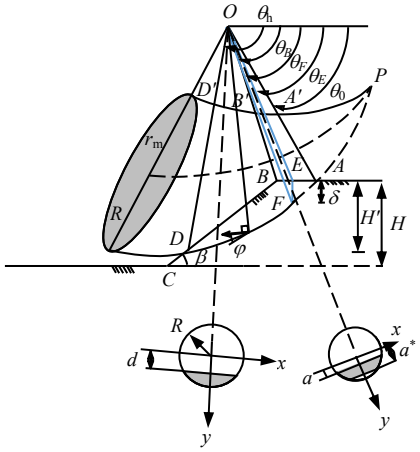

(a) Horn-shape sliding surface (face failure)

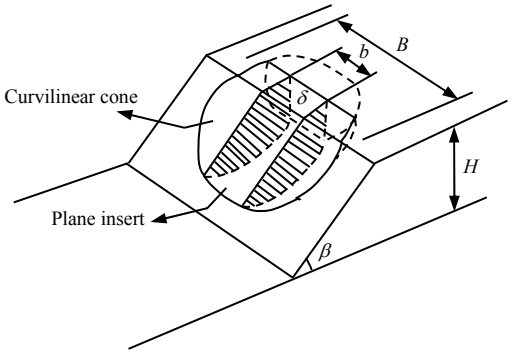

(b) Three-dimensional sliding surface (face failure)

Fig. 4 Three-dimensional face failure mechanism with crack

Michalowski et al.[6] has described R, r_m and the linear velocity at any point on the sliding surface of slope v in the horn-shape log-spiral three-dimensional failure mechanism, which will not be repeated in this paper. Based on the upper bound theory of limit analysis, the upper bound solution can be obtained by establishing the energy balance equation. It is assumed that the soil below the sliding surface remains stable and the sliding mass rotates in a rigid block motion type. In this paper only the work rate done by the soil weight in the sliding mass is considered as the work rate of external force. Referring to the extended study of Gao et al.[7] on the failure mechanism of three-dimensional slopes, the calculation method for the work rate of soil weight W_γ and the work rate of energy dissipation D is provided, the calculation formulas of the work rate of soil weight W_γ and the work rate of energy dissipation D can be obtained by introducing the crack δ. The relevant derivation process and calculation principles of W_γ and D are detailed in the literature[6].

The slope sliding mass includes the plane insert b and the curvilinear cone at the two ends, which should be calculated separately in the calculation process.

The work rate of soil weight for the curvilinear cone W_γ^{curve} is

$$W_\gamma^{\text{curve}} = W_\gamma^{FB} + W_\gamma^{BD} + W_\gamma^{EF} \tag{4}$$

where the derivation process of W_γ^{FB} and W_γ^{BD} is detailed in the literature[7]; and W_γ^{EF} can be expressed as

$$W_\gamma^{EF} = 2\omega\gamma\left[\int_{\theta_E}^{\theta_F}\int_0^{\sqrt{R^2-a^2}}\int_a^{\sqrt{R^2-x^2}}(r_m+y)^2\cos\theta\mathrm{d}y\mathrm{d}x\mathrm{d}\theta - \int_{\theta_E}^{\theta_F}\int_0^{\sqrt{R^2-a^{*2}}}\int_{a^*}^{\sqrt{R^2-x^2}}(r_m+y)^2\cos\theta\mathrm{d}y\mathrm{d}x\mathrm{d}\theta\right] \tag{5}$$

The calculation of the plane insert can be regarded as the extension of the two-dimensional log-spiral mechanism along the width of the slope crest. Therefore, multiplying by the width b is the result of this part. Based on the principle of virtual work, the work rate of soil weight for the plane insert is deduced as

$$W_\gamma^{\text{plane}} = b\omega\gamma\left[\int_{\theta_F}^{\theta_B}\int_a^R(r_m+y)^2\cos\theta\mathrm{d}y\mathrm{d}\theta + \int_{\theta_B}^{\theta_h}\int_d^R(r_m+y)^2\cos\theta\mathrm{d}y\mathrm{d}\theta + \int_{\theta_E}^{\theta_F}\int_a^R(r_m+y)^2\cos\theta\mathrm{d}y\mathrm{d}\theta - \int_{\theta_E}^{\theta_F}\int_{a^*}^R(r_m+y)^2\cos\theta\mathrm{d}y\mathrm{d}\theta\right] \tag{6}$$

The crack is known to exist in advance and there is no energy dissipation. Hence, only the crack structural surface is considered as the sliding mass surface other than the failure surface, and only the energy dissipation on the outer surface of the sliding mass (the slope top *EB*, the slope face *BD* and the crack surface *EF*) is calculated. The derivation process is detailed in the literature[6]. For loess slopes with internal friction angle $\varphi > 0°$, the work rate of energy dissipation for the curvilinear cone D^{curve} is

$$D^{\text{curve}} = D^{EB} + D^{BD} + D^{EF} \tag{7}$$

where the derivation process of D^{EB} and D^{BD} is detailed in the literature[7]; and the expression of D^{EF} is

$$D^{EF} = \frac{2c\omega r_0^2}{\tan\varphi}\left(\frac{\sin^2\theta_0}{\tan^2\theta_E}\int_{\theta_E}^{\theta_F}\frac{\sin\theta}{\cos^3\theta}\sqrt{R^2-a^{*2}}\mathrm{d}\theta\right) \tag{8}$$

The energy dissipation rate of the plane insert D^{plane} is

$$D^{\text{plane}} = \frac{bc\omega r_0^2}{\tan\varphi}\left\{(-\sin^2\theta_0)\int_{\theta_E}^{\theta_B}\frac{\cos\theta}{\sin^3\theta}\mathrm{d}\theta\mathrm{e}^{i\theta} + [-\sin^2(\beta+\theta_h)]\mathrm{e}^{2(\theta_h-\theta_0)\tan\varphi}\int_{\theta_B}^{\theta_h}\frac{\cos(\theta+\beta)}{\sin^3(\theta+\beta)}\mathrm{d}\theta + \left(\frac{\sin^2\theta_0}{\tan^2\theta_E}\right)\int_{\theta_E}^{\theta_F}\frac{\sin\theta}{\cos^3\theta}\mathrm{d}\theta\right\} \tag{9}$$

where ω is the angular velocity; c is the soil cohesion; φ is the soil friction angle; γ is the soil unit weight, β is the slope inclination; R is the mean radius of the horn-shape failure mechanism; r_m is the mean radius of the two log-spirals; and the variables a, d, a^* and the angles θ_0, θ_B, θ_h, θ_F, θ_E can be obtained from the geometric relationship shown in Fig. 4, and more specifically,

$$a = \frac{r_0\sin\theta_0}{\sin\theta} - r_m \tag{10}$$

$$d = \frac{\sin(\theta_h+\beta)}{\sin(\theta+\beta)}\mathrm{e}^{(\theta_h-\theta_0)\tan\varphi}r_0 - r_m \tag{11}$$

$$a^* = \frac{\sin\theta_0}{\cos\theta\tan\theta_E}r_0 - r_m \tag{12}$$

$$\theta_B = \arctan\frac{\sin\theta_0}{\cos\theta_0 - A} \tag{13}$$

$$\theta_E = \arctan\frac{\sin\theta_0}{\mathrm{e}^{(\theta_F-\theta_0)\tan\varphi}\cos\theta_F} \tag{14}$$

$$A = \frac{\sin(\theta_h-\theta_0)}{\sin\theta_h} - \frac{\sin(\theta_h+\beta)}{\sin\theta_h\sin\beta}\left[\sin\theta_h\mathrm{e}^{(\theta_h-\theta_0)\tan\varphi} - \sin\theta_0\right] \tag{15}$$

3.2 Base failure mechanism

For the base failure mechanism of three-dimensional loess slopes with cracks, the angle β' can be introduced to determine the sliding surface, as shown in Fig. 5. When $\beta' = \beta$, the toe failure mechanism of three-dimensional cracked slopes is a special case of the three-dimensional base failure mechanism. Compared with the face failure mechanism, it can be seen that the base failure needs to calculate the dissipated work rate generated by the rotation of the bottom part *CD*. According to the extended calculation method for W_γ and D of the three-dimensional failure mechanism proposed by Gao et al.[7], the calculation formula of W_γ and D for three-dimensional loess slopes with cracks can be deduced.

Similar to the face failure mechanism, the work rate of soil weight for the curvilinear cone W_γ^{curve} is

$$W_\gamma^{\text{curve}} = W_\gamma^{FB} + W_\gamma^{BC} + W_\gamma^{CD} + W_\gamma^{EF} \tag{16}$$

where the derivation process of W_γ^{FB}, W_γ^{BC} and W_γ^{CD} is detailed in the literature[7]; and W_γ^{EF} can be expressed as

$$W_\gamma^{EF} = 2\omega\gamma\left[\int_{\theta_E}^{\theta_F}\int_0^{\sqrt{R^2-a^2}}\int_a^{\sqrt{R^2-x^2}}(r_m+y)^2\cos\theta\mathrm{d}y\mathrm{d}x\mathrm{d}\theta - \int_{\theta_E}^{\theta_F}\int_0^{\sqrt{R^2-a^{*2}}}\int_{a^*}^{\sqrt{R^2-x^2}}(r_m+y)^2\cos\theta\mathrm{d}y\mathrm{d}x\mathrm{d}\theta\right] \tag{17}$$

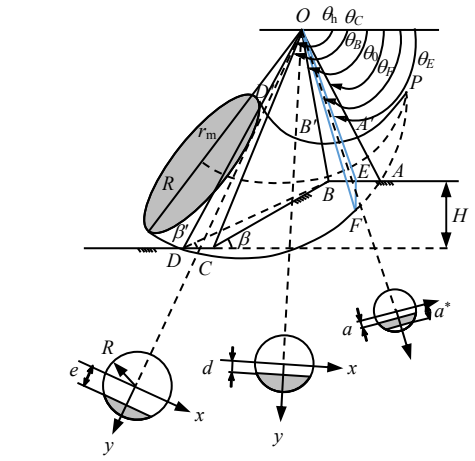

(a) Horn-shape sliding surface (base failure)

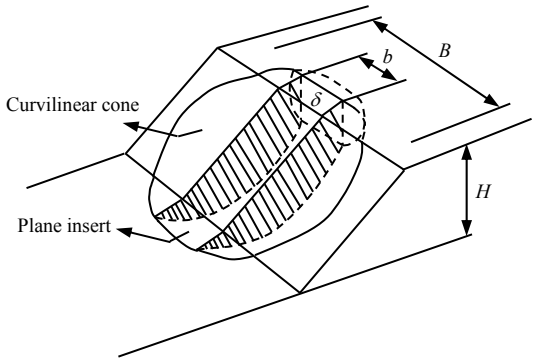

(b) Three dimensional sliding surface (base failure)

Fig. 5 Three-dimensional base failure mechanism with crack

Similarly, the work rate of soil weight for the plane insert W_γ^{plane} is

$$\begin{aligned}W_\gamma^{\text{plane}} = b\omega\gamma\Big[&\int_{\theta_F}^{\theta_B}\int_a^R (r_m+y)^2\cos\theta\mathrm{d}y\mathrm{d}\theta+\\&\int_{\theta_B}^{\theta_C}\int_d^R (r_m+y)^2\cos\theta\mathrm{d}y\mathrm{d}\theta+\\&\int_{\theta_C}^{\theta_h}\int_e^R (r_m+y)^2\cos\theta\mathrm{d}y\mathrm{d}\theta+\\&\int_{\theta_E}^{\theta_F}\int_a^R (r_m+y)^2\cos\theta\mathrm{d}y\mathrm{d}\theta-\\&\int_{\theta_E}^{\theta_F}\int_{a^*}^R (r_m+y)^2\cos\theta\mathrm{d}y\mathrm{d}\theta\Big]\end{aligned} \tag{18}$$

Similarly, for loess slopes with $\varphi>0°$, the work rate of energy dissipation for the curvilinear cone D^{curve} is

$$D^{\text{curve}} = D^{EB}+D^{BC}+D^{CD}+D^{EF} \tag{19}$$

where the derivation process of D^{EB}, D^{BC} and D^{CD} is detailed in the literature[7]; and the expression of D^{EF} is

$$D^{EF} = \frac{2c\omega r_0^{\prime 2}}{\tan\varphi}\left(\frac{\sin^2\theta_0}{\tan^2\theta_E}\int_{\theta_E}^{\theta_F}\frac{\sin\theta}{\cos^3\theta}\sqrt{R^2-a^{*2}}\mathrm{d}\theta\right) \tag{20}$$

Similarly, the energy dissipation rate of the plane insert D^{plane} is

$$\begin{aligned}D^{\text{plane}} = \frac{bc\omega r_0^{\prime 2}}{\tan\varphi}\Bigg\{&(-\sin^2\theta_0)\int_{\theta_E}^{\theta_B}\frac{\cos\theta}{\sin^3\theta}\mathrm{d}\theta+\\&\left[\frac{-\sin^2(\beta+\theta_C)\sin^2\theta_h}{\sin^2\theta_C}\mathrm{e}^{2(\theta_h-\theta_0)\tan\varphi}\int_{\theta_B}^{\theta_C}\frac{\cos(\theta+\beta)}{\sin^3(\theta+\beta)}\mathrm{d}\theta\right]+\\&\left(-\sin^2\theta_h\mathrm{e}^{2(\theta_h-\theta_0)\tan\varphi}\int_{\theta_C}^{\theta_h}\frac{\cos\theta}{\sin^3\theta}\mathrm{d}\theta\right)+\\&\left(\frac{\sin^2\theta_0}{\tan^2\theta_E}\right)\int_{\theta_E}^{\theta_F}\frac{\sin\theta}{\cos^3\theta}\mathrm{d}\theta\Bigg\}\end{aligned} \tag{21}$$

where the variables a and a^* and the angle θ_E are consistent with the expression of face failure mechanism; and the variables d and e and the angles θ_B and θ_C can be obtained from the geometrical relationship in Fig. 5, specifically as

$$d = \frac{\sin(\theta_C+\beta)\sin\theta_h}{\sin(\theta+\beta)\sin\theta_C}\mathrm{e}^{(\theta_h-\theta_0)\tan\varphi}r_0 - r_m \tag{22}$$

$$e = \frac{\sin\theta_h}{\sin\theta}\mathrm{e}^{(\theta_h-\theta_0)\tan\varphi}r_0 - r_m \tag{23}$$

$$\theta_B = \arctan\frac{\sin\theta_0}{\cos\theta_0 - A'} \tag{24}$$

$$\theta_C = \arctan\frac{\sin\theta_h\mathrm{e}^{(\theta_h-\theta_0)\tan\varphi}}{\cos\theta_0 - A' - \dfrac{\sin\theta_h\mathrm{e}^{(\theta_h-\theta_0)\tan\varphi}-\sin\theta_0}{\tan\beta}} \tag{25}$$

$$A' = \frac{\sin(\theta_h-\theta_0)}{\sin\theta_h} - \frac{\sin(\theta_h+\beta')}{\sin\theta_h\sin\beta'}\left[\sin\theta_h\mathrm{e}^{(\theta_h-\theta_0)\tan\varphi}-\sin\theta_0\right] \tag{26}$$

By establishing the energy balance equation (Eq. (27)) between the work rate of curvilinear cone of the sliding mass done by soil weight W_γ^{curve}, the work rate of plane insert done by soil weight W_γ^{plane} and the energy dissipation rate of curvilinear cone D^{curve}, the energy dissipation rate of insert plane D^{plane}, upper bound solution in the kinematic state based on the limit analysis can be obtained

$$W_\gamma^{\text{curve}} + W_\gamma^{\text{plane}} = D^{\text{curve}} + D^{\text{plane}} \tag{27}$$

4 Program optimization and numerical results

The energy balance Eq. (27) is established based on the face failure mechanism and base failure mechanism constructed by the limit analysis method, and the expression of the dimensionless critical height $\gamma H/c$ of three-dimensional loess slopes with cracks is obtained. The critical height $\gamma H/c$ is a function of variables θ_0, θ_h, θ_F, r_0'/r_0 and b/H. In order to obtain the upper bound solution of the critical height, the minimum value of each variable needs to be calculated optimally. Because of the difficulty and the tendency to fall into local minima when optimizing

multiple parameters, the random search method proposed by Chen[14] is used in this paper. This method has been well validated in relevant published literature and is a very effective optimization search method[7, 15−16]. In view of the calculation formulas derived from the face failure mechanism and the base failure mechanism, Matlab software is used to program for numerical calculation[17−18]. To make the slope failure mechanism conform to the geometric boundary conditions, the above parameters should meet the conditions:

$$\left.\begin{aligned} &0<\theta_0<\theta_F<\theta_{\mathrm{h}}<\pi \\ &0<r_0'/r_0<1 \\ &0<\frac{b}{H}<\frac{B}{H} \end{aligned}\right\} \tag{28}$$

For each parameter needed to be optimized, the minimum critical height $\gamma H/c$ can be obtained by iterative calculation with a given initial value, initial search step and accuracy requirement. In the process of optimization programming, the accuracy of the angle is set to 0.01°, and the accuracy of the ratio is set to 0.001. In order to verify the correctness of the formulas derived in this paper for calculating the critical height of three-dimensional loess slopes with cracks under different failure modes, the upper bound solution of critical height $\gamma H/c$ is obtained by selecting the vertical slope ($\beta=90°$), the crack depth $\delta=0$ and $n=1$ or $\beta'=\beta$ for the failure mechanism.

As can be seen from Table 1, the critical height values obtained from the formulas derived in this paper are in good agreement with those obtained by Gao et al.[7] and He et al.[8]. Due to different numerical integration algorithms in coding and different restricted conditions, the results of the critical height may produce some errors, but the errors are within the acceptable range. Therefore, the comparison results show that the theoretical calculating formulas derived in this paper for the failure mechanism of three-dimensional cracked loess slopes are valid and feasible.

Table 1 Comparison of critical height (vertical slope, δ=0, n =1)

φ/(°)	B/H	θ_0/(°)	θ_{h}/(°)	r_0'/r_0	b/H	$\gamma H/c$			
						This study	Michalowski et al.[6]	Gao et al.[7]	He et al.[8]
15	1.5	23.23	59.48	0.546	0.527	6.735	7.124	6.783	6.772
15	5.0	31.95	61.23	0.579	3.846	5.457	5.504	5.456	5.456
30	0.8	16.06	60.15	0.707	0.100	12.668	14.368	12.263	12.260
30	3.0	38.61	66.30	0.607	1.881	7.645	7.974	7.632	7.630

According to the equations derived in this paper, the critical height of toe failure in the presence of the most unfavorable crack at different internal friction angles φ and slope inclinations β is analyzed respectively. As shown in Fig. 6, the least upper bound solution of critical height $\gamma H/c$ with respect to different crack depths δ/H is obtained. It can be found that when the constraint width B/H varies from 0.8 to infinity (under plane strain mechanism), the critical height tends to decrease with the increase of constraint width. As the crack depth increases, the upper bound value of critical height gradually reduces. When the crack depth reaches a specific value, the critical height approaches a fixed value, i.e., the critical crack depth value $(\delta/H)_{\min}$. By comparing Figs. 6(a) and 6(b), it is found that the critical crack depth increases with the increase of slope inclination β. Comparing Figs. 6(a) and 6(c) shows that the critical crack depth decreases with the increase of internal friction angle φ. The results indicate that the constraint width, slope inclination and internal friction angle have certain effects on the critical crack depth of loess slopes. The infinite constraint width (plane strain mechanism) exhibits minimum critical height and critical crack depth values compared with the finite constraint width (three-dimensional slope), which further demonstrates the three-dimensional effect.

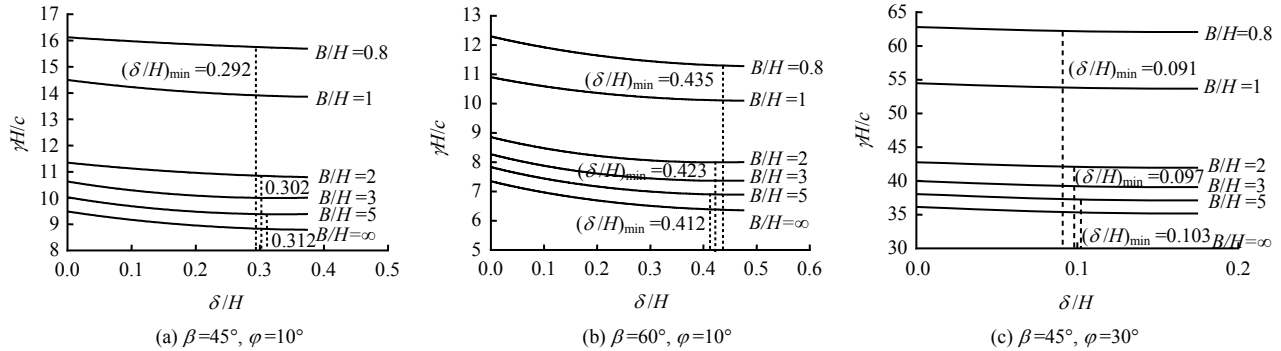

(a) β=45°, φ=10° (b) β=60°, φ=10° (c) β=45°, φ=30°

Fig. 6 Critical height of slopes with different crack depths

It can be seen by comparing Table 2 and Table 3 that the three-dimensional loess slopes with pre-existing cracks exhibit lower critical height values compared to intact slopes, indicating that the presence of crack leads to a reduction in the loess slope stability. As evident in Fig. 7, the failure of loess slopes with pre-existing cracks in most cases is of toe failure mechanism. The critical height value decreases gradually with the increase of slope inclination. With the same slope inclination, the critical height value decreases with the increase of the constraint width value, and reaches the lowest under the plane strain mechanism (two-dimensional). Comparing Figs. 7(a) and 7(b) demonstrates that the critical height value increases as the internal friction angle φ increases, indicating that the stability of loess slopes is improved with the increase of internal friction angle φ. When the constraint width is small (B/H <0.8), the failure mechanism of cracked loess slopes is mostly the face failure mechanism, where the slope failure mechanism changes gradually from the face failure to the toe failure as the slope inclination β increases when the constraint width $B/H=0.6$ and 0.8 and the internal friction angle φ=15° and 10°. It shows that the constraint width and the internal friction angle have some influence on the failure mechanism of three-dimensional loess slopes.

Analysis of Table 2 reveals that for loess slopes with internal friction angle $\varphi=15°$ and slope inclination β=30°, the crack depths are almost close to 0 for small constraint widths of $B/H=0.5$, 0.6 and 0.8, and the critical height values are similar to those of slopes without cracks. Therefore, for three-dimensional cracked loess slopes with the constraint width $B/H \leqslant 0.8$ and $\beta \leqslant 30°$, the crack at the crest of the slope can be approximately ignored. As shown in Figs. 8(a) and 8(b), under certain constraint widths, the crack depth gradually decreases as the friction angle φ increases, and the position of the crack gradually approaches slope shoulder. With the increase of slope inclination β, the crack depth increases, and the location of the crack is gradually far from the slope shoulder, indicating that the slope inclination can affect the development of crack depth.

Table 2 Values of critical height $\gamma H/c$ (φ=15°)

B/H	Literature resource	β=30°		β=45°		β=60°		β=75°	
		$\gamma H/c$	δ/H	$\gamma H/c$	δ/H	$\gamma H/c$	δ/H	$\gamma H/c$	δ/H
0.5	This study	73.340	0.099	33.240	0.199	23.783	0.323	18.264	0.495
	The study of Gao et al.[7]	73.156	—	32.371	—	21.512	—	16.580	—
0.6	This study	61.438	0.079	26.857	0.209	17.642	0.313	12.013	0.585
	The study of Gao et al.[7]	61.014	—	26.913	—	17.765	—	13.727	—
0.8	This study	46.032	0.073	20.012	0.222	13.857	0.337	10.548	0.428
	The study of Gao et al.[7]	46.101	—	21.223	—	14.338	—	11.074	—
1.0	This study	39.131	0.119	18.519	0.227	12.374	0.270	9.391	0.497
	The study of Gao et al.[7]	38.011	—	18.653	—	12.831	—	9.784	—
2.0	This study	27.789	0.126	14.146	0.233	9.667	0.364	6.475	0.383
	The study of Gao et al.[7]	28.098	—	14.699	—	10.363	—	7.997	—
5.0	This study	23.347	0.113	12.257	0.257	8.363	0.334	6.220	0.521
	The study of Gao et al.[7]	23.821	—	12.973	—	9.251	—	7.063	—

Table 3 Values of critical height $\gamma H/c$ (φ=30°)

B/H	Literature resource	β=45°		β=60°		β=75°	
		$\gamma H/c$	δ/H	$\gamma H/c$	δ/H	$\gamma H/c$	δ/H
0.5	This study	97.004	0.059	40.765	0.157	25.147	0.348
	The study of Gao et al.[7]	96.829	—	40.801	—	25.988	—
0.6	This study	72.747	0.122	33.674	0.180	20.807	0.364
	The study of Gao et al.[7]	80.678	—	33.999	—	21.572	—
0.8	This study	61.873	0.092	26.822	0.208	16.242	0.400
	The study of Gao et al.[7]	62.213	—	26.486	—	16.659	—
1.0	This study	54.042	0.109	23.212	0.224	14.266	0.453
	The study of Gao et al.[7]	54.193	—	23.413	—	14.461	—
2.0	This study	42.133	0.098	18.018	0.215	11.486	0.444
	The study of Gao et al.[7]	42.625	—	18.941	—	11.844	—
5.0	This study	37.480	0.099	16.362	0.241	9.461	0.419
	The study of Gao et al.[7]	37.966	—	17.051	—	10.610	—

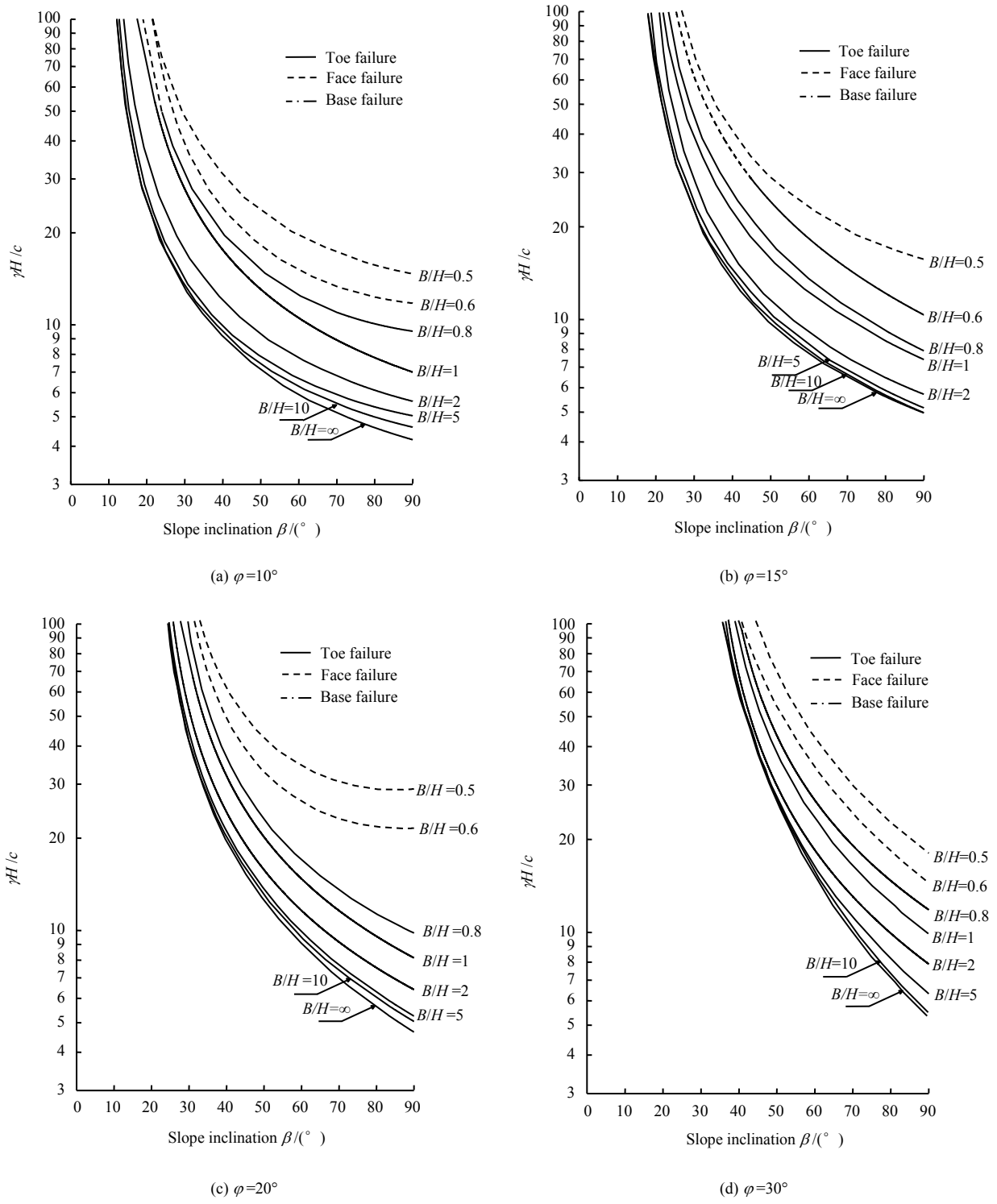

(a) φ=10° (b) φ=15°

(c) φ=20° (d) φ=30°

Fig. 7 Critical height of cracked slopes with different values of *B*/*H*

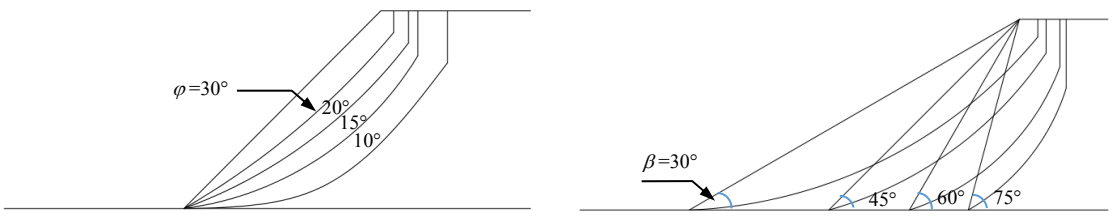

(a) β=45°，B/H=1.0 (b) φ=20°，B/H=1.0

Fig. 8 Effect of internal friction angle and slope angle on the crack depth under 3D condition

5 Conclusion

Based on the horn-shape three-dimensional rotational failure mechanism, the study adopts the upper bound limit analysis to obtain the upper bound solution of critical height through the random search method, and analyzes the stability of three-dimensional loess slopes with a vertical crack under different failure mechanisms. The conclusions can be drawn as follows:

(1) A pre-existing vertical crack is introduced, the energy balance equation is established based on the upper bound limit analysis to obtain the dimensionless expression of critical height $\gamma H / c$ under different failure mechanisms for three-dimensional cracked loess slopes, and the slope stability is analyzed.

(2) In the toe failure mechanism, the critical height decreases with the increase of constraint width. Under the same constraint width B / H, the critical height does not change as it reduces to the critical crack depth, indicating that the critical crack depth will no longer affect the critical height when the crack depth is greater than the critical crack depth. The critical crack depth $(\delta / H)_{\min}$ increases with the increase of slope inclination β and decreases with the increase of friction angle φ.

(3) Most three-dimensional cracked loess slope failure mechanisms are of the failure mechanism. When the constraint width is $B / H < 0.8$, it belongs to face failure. When the friction angle is small, as the constraint width reduces, the slope failure mechanism gradually transits from the face failure mechanism to the toe failure mechanism. It can be seen that the constraint width and the friction angle can affect the slope failure mechanism. Compared with intact slopes, the critical height of loess slopes with vertical cracks is smaller, which indicates that the existence of vertical cracks has a specific impact on the loess slope stability.

References

[1] CHEN Zu-yu. Limit analysis for the classic problems of soil mechanics[J]. Chinese Journal of Geotechnical Engineering, 2002, 24(1): 1−11.

[2] UTILI S. Investigation by limit analysis on the stability of slopes with cracks[J]. Géotechnique, 2013, 63(2): 140−154.

[3] CHEN W F. Limit analysis and soil plasticity[M]. Rotterdam, Netherlands: Elsevier, 1975.

[4] SPENCER E. A method of analysis of the stability of embankments assuming parallel inter-slice forces[J] Géotechnique, 1967, 17(1): 11−26.

[5] MICHALOWSKI R L. Cracks in slopes: limit analysis approach to stability assessment[C]//GeoCongress 2012: State of the Art and Practice in Geotechnical Engineering. Oakland, California: ASCE, 2012: 442−450.

[6] MICHALOWSKI R L, DRESCHER A. Three-dimensional stability of slopes and excavations[J]. Geotechnique, 2009, 59(10): 839−850.

[7] GAO Y, ZHANG F, LEI G, et al. An extended limit analysis of three-dimensional slope stability[J]. Géotechnique, 2013, 63(6): 518−524.

[8] HE Y, LIU Y, ZHANG Y B, et al. Stability assessment of three-dimensional slopes with cracks[J]. Engineering Geology, 2019, 252: 136−144.

[9] HE Yi, YU Jun-yan, YUAN Ran, et al. Stability analysis of soil slope with cracks considering upper slope inclination angle[J]. China Journal of Highway and Transport, 2021, 34(5): 45−54.

[10] LI Z, YANG X L, LI T. Static and seismic stability assessment of 3D slopes with cracks[J]. Engineering Geology, 2019, 265: 105450.

[11] RAO Ping-ping, WU Jian, CUI Ji-fei, et al. Extended three-dimensional analysis of cracked slopes using upper-bound limit analysis method[J]. Chinese Journal of Geotechnical Engineering, 2021, 43(9): 1612-1620.

[12] CHEN Zu-yu. Stability analysis of soil slope: principle, method and procedure[M]. Beijing: China Water & Power Press, 2003.

[13] ZHOU Zhi-jun, ZHU Lin-xuan, CHEN Lei. Calculation method of vertical crack depth of loess slope with inclined crest[J]. China Journal of Highway and Transport, 2021, 34(5): 37−44.

[14] CHEN Z Y. Random trials used in determining global minimum factors of safety of slopes[J]. Canadian Geotechnical Journal, 1992, 29(2): 225−233.

[15] LEI Guo-hui, ZHANG Hui-min, LIU Fang-xue, et al. Plasticity limit analysis of stability of embankment fill on layered soft soil ground[J]. Chinese Journal of Geotechnical Engineering, 2018, 40(8): 1522−1527.

[16] WANG Di, WANG Hong-quan, WANG Xiao-fei, et al. Stability analysis of double layer soil slope based on limit analysis[J]. Journal of Water Resources and Architectural Engineering, 2020, 18(4): 209−214.

[17] TANG Gao-peng, ZHAO Lian-heng, LI Liang, et al. Program development for slope stability using MATLAB software and upper bound limit analysis[J]. Rock and Soil Mechanics, 2013, 34(7): 2091−2098.
WANG Lu-lu, PAN Qiu-jing, YANG Xiao-li. Dynamic upper bound limit analysis for cohesive three-dimensional soil slopes[J]. Journal of Railway Science and Engineering, 2013, 10(2): 87−89.